Supporting Information for: Cl_2^- chemical ionization mass spectrometry (Cl_2-CIMS) for the measurement of acyl peroxy radicals

Tyson C. Berg[1], Michael F. Link[1,†], Delphine K. Farmer[1,*]

[1]Department of Chemistry, Colorado State University, Fort Collins, Colorado 80523, United States

[†]Present address: Engineering Laboratory, National Institute of Standards and Technology, Gaithersburg, Maryland 20899, USA.

*Corresponding author: Delphine K. Farmer- Department of Chemistry, Colorado State University, Fort Collins, Colorado 80253, United States. Email: delphine.farmer@colostate.edu

Contents

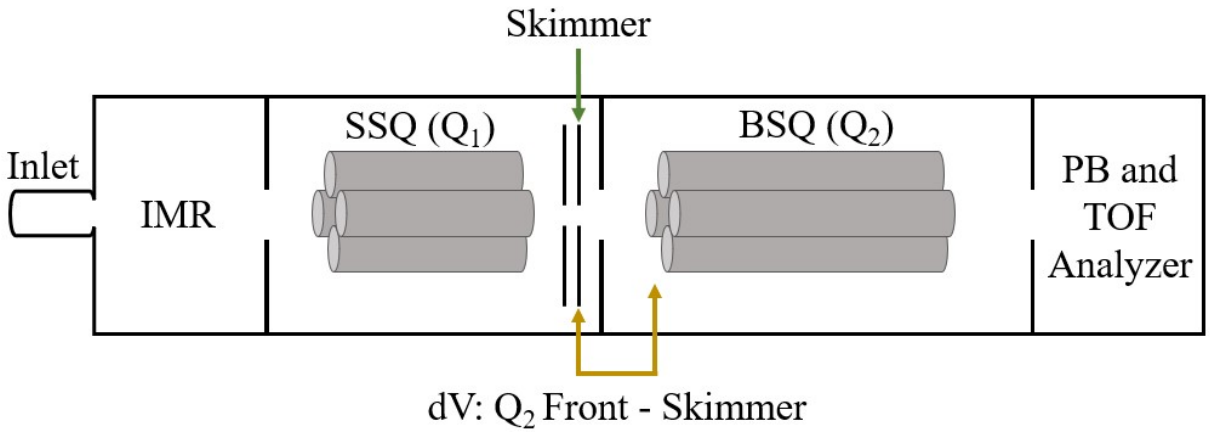

Figure S1. Simplified diagram of the CIMS ion optics, including the ion-molecule reactor (IMR), short-segment quadrupole (SSQ), big-segment quadrupole (BSQ), primary beam (PB) and time-of-flight (TOF) mass analyzer segments (with PB and TOF segments combined for simplicity). During voltage scanning experiments, we altered the voltage difference (dV) between the front of the BSQ and the up-flow skimmer plate. For each voltage step, the skimmer plate voltage and the voltage settings of up-flow components were altered by the same amount to maintain constant dVs between adjacent components. The Q_2 Front and down-flow components remained unchanged across the dV scan steps. We maintained IMR total pressure of 65 mbar and water vapor pressure of 0.5 mbar for dV scan experiments. Normal operating dV was 1.4 V.

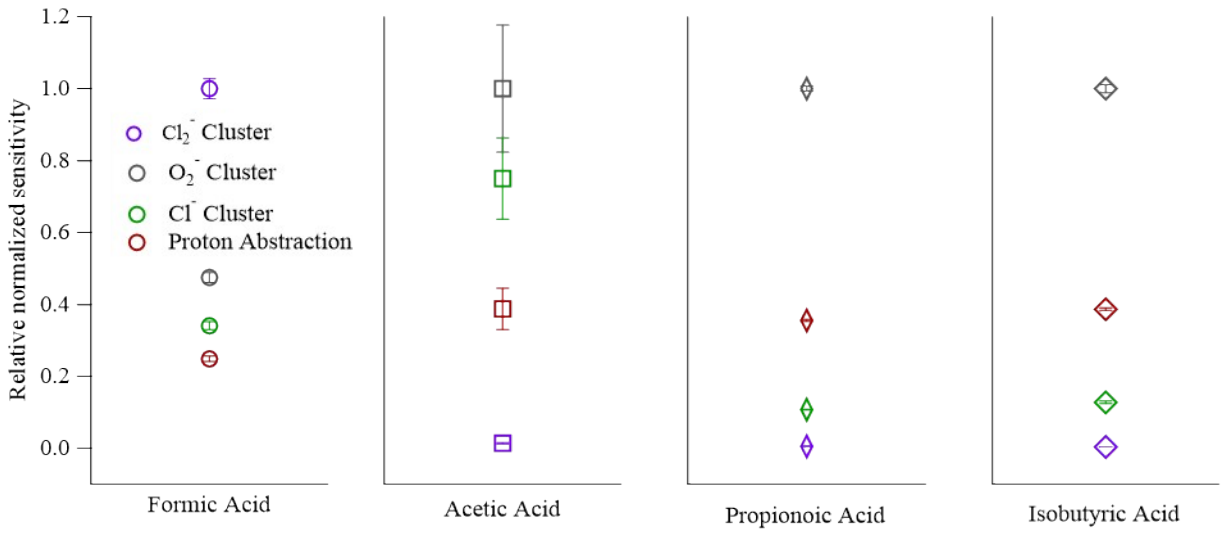

Figure S2. Cl_2-CIMS sensitivities to examined organic acids. Sensitivities to various product ions at set relative to the most sensitive ion.

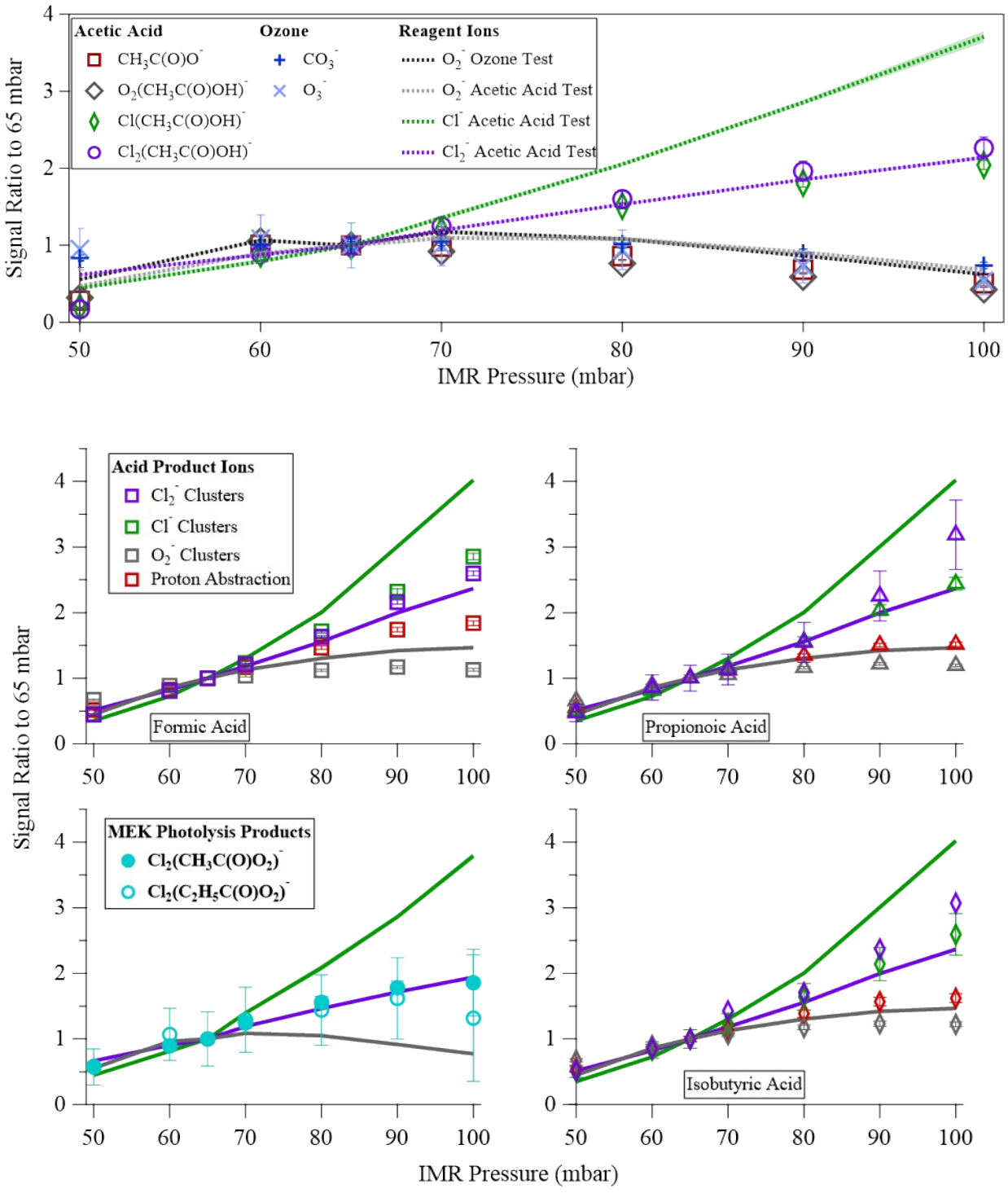

Figure S3. Analyte ion signal responses to IMR pressure change (50 to 100 mbar), with background reagent ion counts at each pressure setting included (lines). During pressure change tests, we maintained IMR water vapor pressures of ca. 0.5 mbar and dV = 1.4 V between the skimmer and BSQ front. Error bars represent standard deviation of the signal average at each step. $Cl_2(C_3H_7C(O)OH)^-$ error bars not included for ease of visualization.

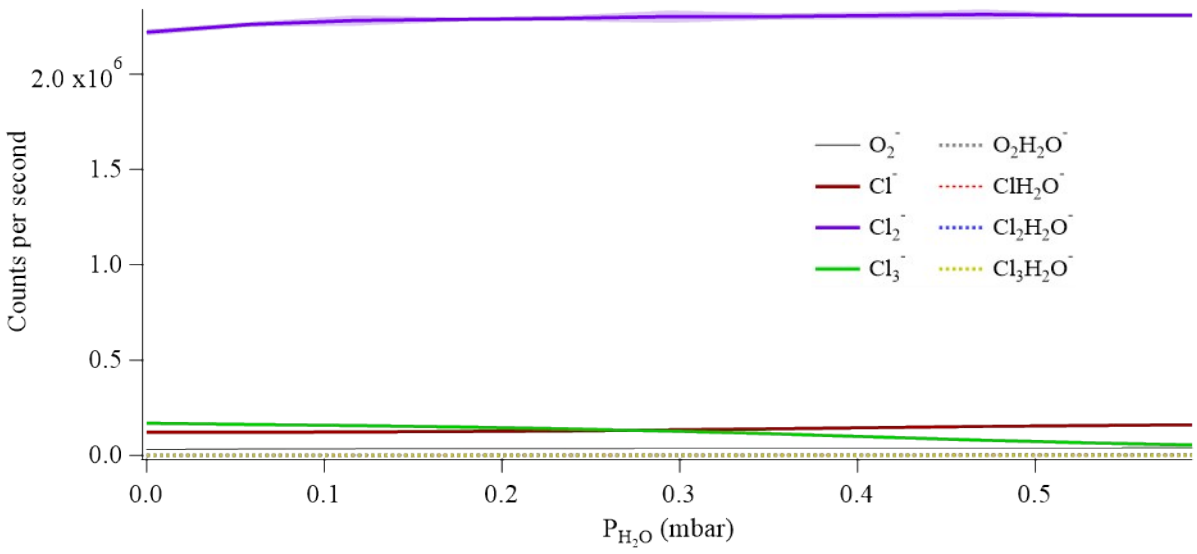

Figure S4. Reagent ion response to changes in the ion-molecule reactor water vapor pressure. During water vapor pressure modulation, we maintained IMR pressure of 65 mbar and dV = 1.4 V between the skimmer and BSQ front.

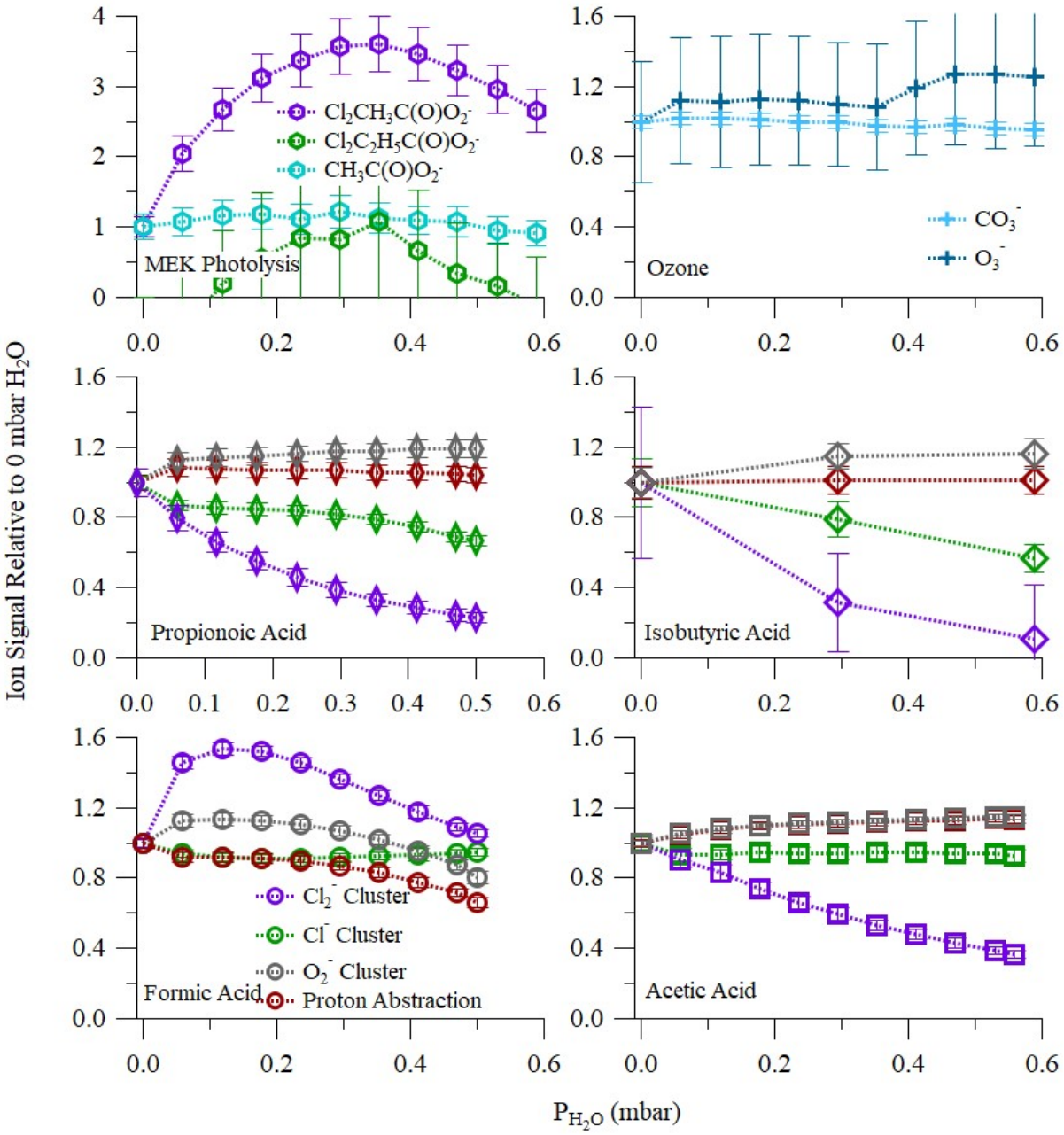

Figure S5. Data for ion-molecule reactor water vapor pressure impacts on analyte ion signal. Ion signal for each vapor pressure setting relative to signal from dry ion-molecule reactor. The influence of water vapor pressure on analyte detection was much larger than the observed impact on reagent ion signals. These impacts were also largest for Cl_2^- clusters and generally small (±20%) for ions that resulted from reaction with O_2^-.

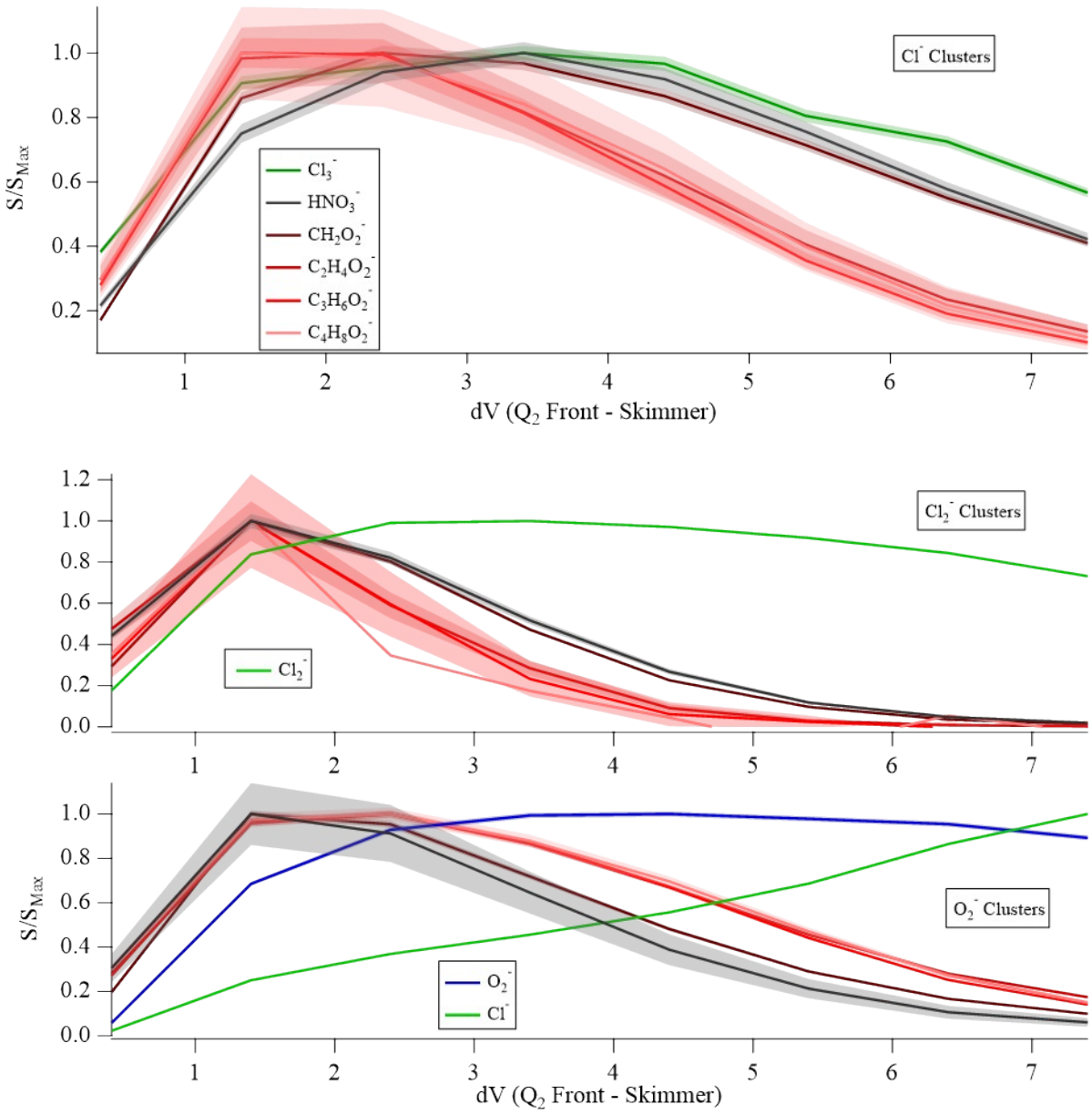

Figure S6. dV scan data for the examined organic acids and HNO_3 (*see Figure S12 for information on the HNO_3 source and HNO_3 use in specific supplemental tests)*. (Upper) During dV scan tests of select standards, the dV_{50} for all Cl^- clusters was achieved at or below dV=~7.5, while the Cl_3^- dV_{50} exists somewhere slightly above this. This result suggests that Cl_3^- has a greater binding energy than Cl^- cluster binding energy with observed analyte ions and Cl^- transfer from Cl_3^- to any of the analytes studied here is unlikely. Included in middle and lower graphs are the Cl_2^- and O_2^- clusters signals across the same set of dV scan tests. Cl^- background signal change is included in with the O_2^- clusters and behaves similarly to the non-cluster analyte ions (H^+ abstraction products; not shown). Shading represents the 1σ SDs for each ion signal but is not shown for $Cl_2(C_4H_8O_2)^-$ for ease of visualization (less than 10 cps at any dV for this ion leads to large relative signal error).

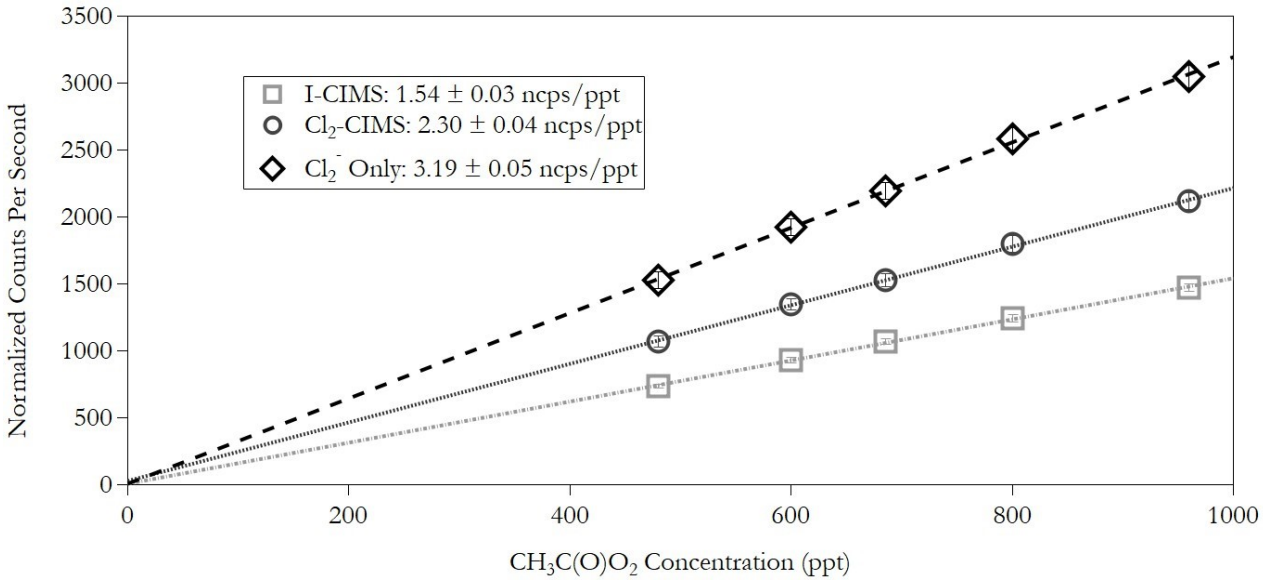

Figure S7 1-minute average signal (background-subtracted and normalized per million reagent ions) for $X(CH_3C(O)O_2)^-$ (X = I or Cl_2) during $CH_3C(O)O_2$ calibrations. Light-gray squares represent $I(CH_3C(O)O_2)^-$ from the I-CIMS. Gray circles show $Cl_2(CH_3C(O)O_2)^-$ from the Cl_2-CIMS normalized to the sum of O_2^-, Cl^-, Cl_2^-, and Cl_3^-. Black diamonds also represent $Cl_2(CH_3C(O)O_2)^-$ but normalized to Cl_2^- only.

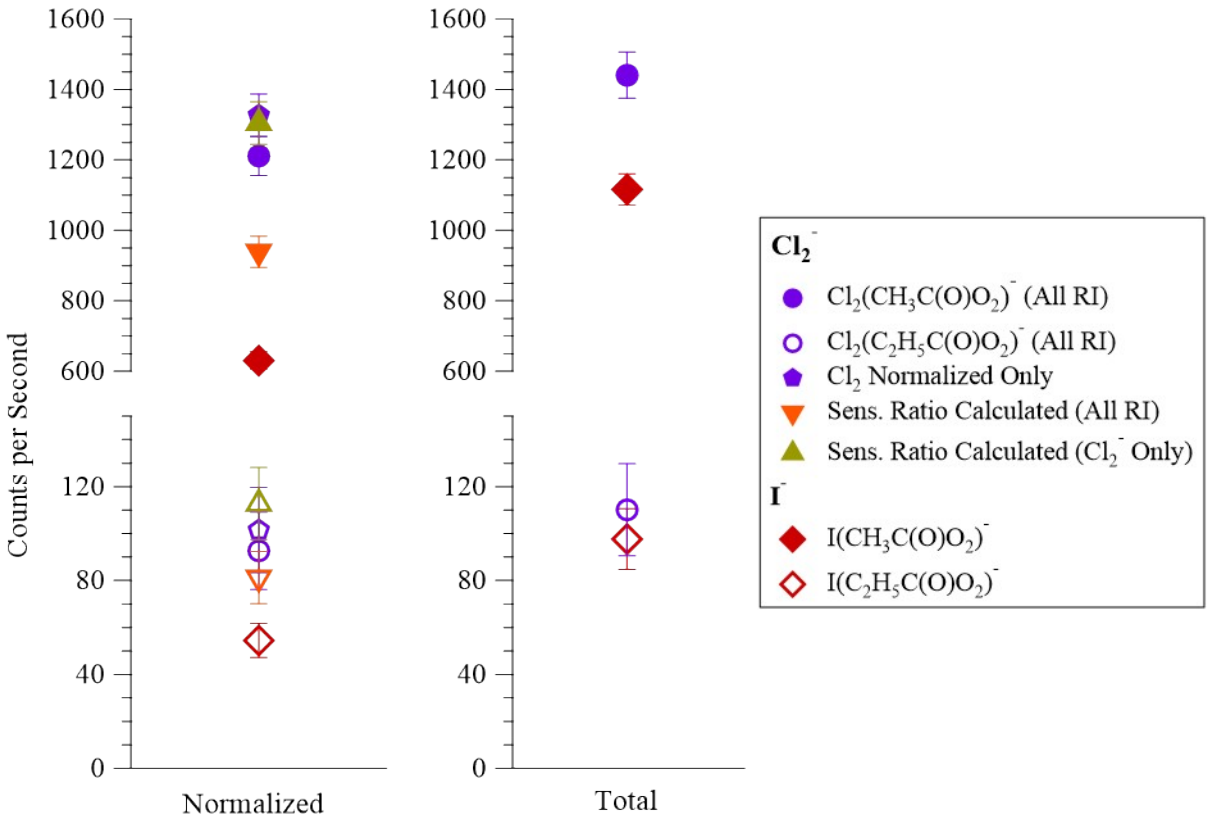

Figure S8. Total (right) and normalized (left) signals from the MEK quantum yield tests (filled markers for $CH_3C(O)O_2$ and open markers for $C_2H_5C(O)O_2$). Cl_2-CIMS signals are shown normalized to total reagent ion signal (All RI; circles on left) and Cl_2^- only (pentagons). We produced expected Cl_2-CIMS signals (Sens. Ratio Calculated) by multiplying the I-CIMS normalized signal and the sensitivity ratios from PAN calibrations (Figure S7). Comparison of actual and expected counts normalized to Cl_2^- shows close agreement, while the expected signal from normalization to all reagent Cl_2-CIMS reagent ions is below the observed signal. This agreement of Cl_2^- normalized $RC(O)O_2$ signal ratios between the MEK photolysis tests and the $CH_3C(O)O_2$ calibrations occurs despite differences in the Cl_2 bulb concentration and age and resulting differences in Cl_2^- contribution to total reagent ion signal. This suggests a direct relationship between Cl_2^- background counts and $Cl_2(RC(O)O_2)^-$ signal across the two tests.

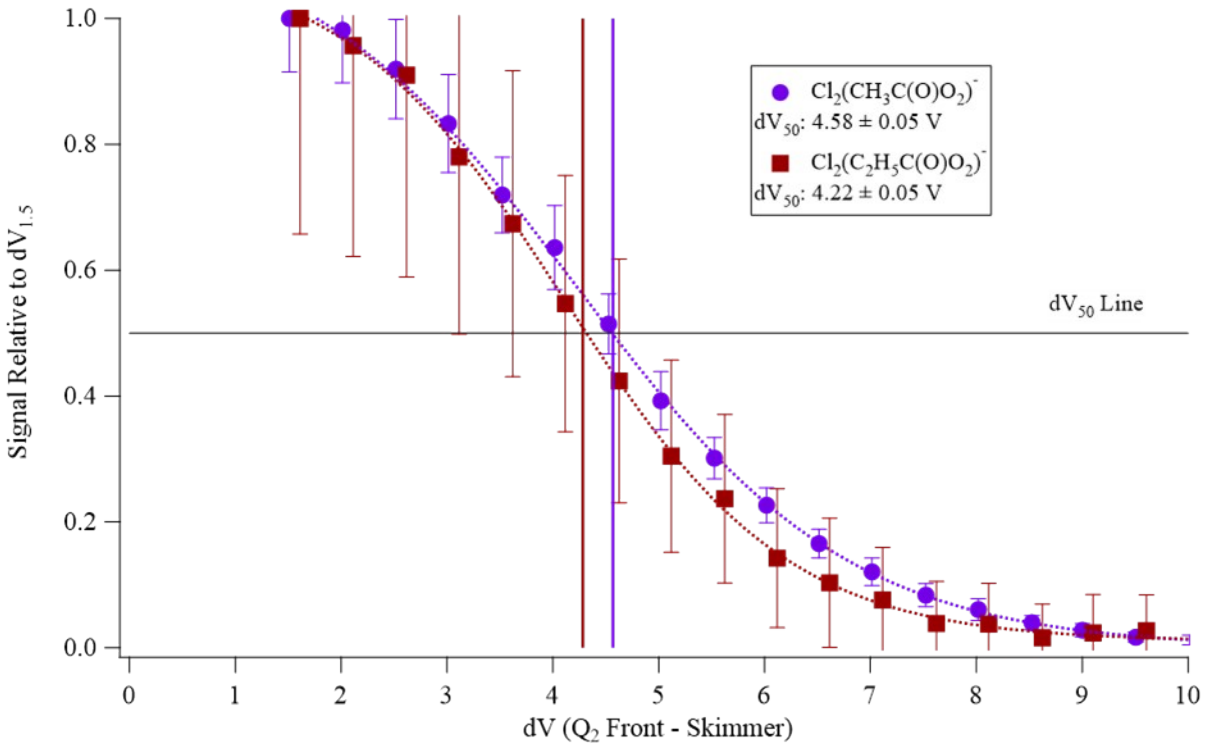

Figure S9. dV scan data for $Cl_2(CH_3C(O)O_2)^-$ and $Cl_2(C_2H_5C(O)O_2)^-$ (ratio relative to dV = ~1.5) measured from MEK photolysis in the photolysis reactor system. Dashed lines represent sigmoidal fits to the analyte signal ratio data and solid vertical lines indicate the position of half-maximum signal in dV-space (dV_{50}). We use the similar dV_{50} values for $Cl_2(CH_3C(O)O_2)^-$ and $Cl_2(C_2H_5C(O)O_2)^-$ observed in this experiment to assume a similar cluster binding energy and, therefore, similar Cl_2^- CIMS sensitivity to $CH_3(O)O_2$ and $C_2H_5C(O)O_2$. $Cl_2(C_2H_5C(O)O_2)^-$ data shifted by +0.2 dV for ease of visibility.

		Reagent Ion							
		O_2^-		Cl^-		Cl_2^-		Cl_3	
Analyte	**Ion**	R^2	*Slope*	R^2	*Slope*	R^2	*Slope*	R^2	*Slope*
Nitric Acid	NO_3^-	0.96	0.26	0.66	-0.97	0.89	-0.70	0.77	-0.03
	$O_2NHO_3^-$	1.00	0.98	0.72	-3.65	0.93	-2.60	0.79	-0.13
	$ClHNO_3^-$	0.99	-0.46	0.73	1.73	0.93	1.23	0.79	0.06
	$Cl_2HNO_3^-$	0.95	-0.32	0.92	1.36	1.00	0.89	0.54	0.03
Formic Acid	$HC(O)O^-$	1.00	1.02	0.93	-2.55	1.00	-1.86	0.72	-0.11
	$O_2HC(O)OH^-$	1.00	1.01	0.92	-2.52	1.00	-1.85	0.74	-0.11
	$ClHC(O)OH^-$	0.92	-0.43	0.68	0.96	0.86	0.76	0.95	0.05
	$Cl_2HC(O)OH^-$	0.92	-0.26	1.00	0.72	0.96	0.50	0.50	0.02
Acetic Acid	$CH_3C(O)O^-$	0.99	1.02	0.90	-2.54	0.98	-1.86	0.74	-0.11
	$O_2CH_3C(O)OH^-$	0.99	1.03	0.91	-2.54	0.98	-1.87	0.74	-0.11
	$ClCH_3C(O)OH^-$	0.99	-0.85	0.95	2.16	1.00	1.56	0.68	0.09
	$Cl_2CH_3C(O)OH^-$	0.75	-0.21	0.94	0.62	0.83	0.41	0.29	0.02
Propanoic Acid	$C_2H_5C(O)O^-$	0.98	1.01	0.95	-3.73	0.99	-2.38	0.67	-0.12
	$O_2C_2H_5C(O)OH^-$	0.98	1.01	0.95	-3.73	0.99	-2.38	0.67	-0.12
	$ClC_2H_5C(O)OH^-$	0.95	-0.42	1.00	1.63	0.98	1.01	0.55	0.04
	$Cl_2C_2H_5C(O)OH^-$	0.52	-0.18	0.74	0.79	0.59	0.44	0.11	0.01
Isobutyric Acid	$C_3H_7C(O)O^-$	0.99	1.03	0.80	-4.23	0.96	-3.29	0.63	-0.12
	$O_2C_3H_7C(O)OH^-$	0.99	1.03	0.80	-4.24	0.96	-3.29	0.63	-0.12
	$ClC_3H_7C(O)OH^-$	0.84	-0.31	0.93	1.50	0.97	1.09	0.35	0.03
	$Cl_2C_2H_5C(O)OH^-$	0.06	0.05	0.05	0.19	0.00	0.00	0.39	-0.02
Ozone	O_3^-	0.99	0.98	0.75	-3.11	0.90	-2.59	0.71	-0.11
	CO_3^-	0.99	0.98	0.75	-3.12	0.90	-2.59	0.70	-0.11
Acetyl Peroxy Radical	$CH_3C(O)O^-$	0.98	0.93	0.77	-5.70	1.00	-3.74	0.72	-0.14
	$CH_3C(O)OO^-$	0.99	0.99	0.75	-6.03	1.00	-3.98	0.73	-0.15
	$Cl_2CH_3C(O)OO^-$	0.30	0.12	0.00	0.02	0.18	-0.36	0.72	-0.03

Table S10. R^2 and slopes for all correlation fits of analyte ions and reagent ion counts presented in Figures 5 and S12. $Cl_2CH_3C(O)OO^-$ data from the initial 40 ppm tank test are shown here. Linear fits of $Cl_2CH_3C(O)OO^-$ data to the retest of Cl_2 concentration correlations with 40 ppm and 10 ppm Cl_2 tanks (Figure S11) returned Slope = 0, R^2 = 0.002 and Slope = 0.53, R^2 = 0.99, respectively.

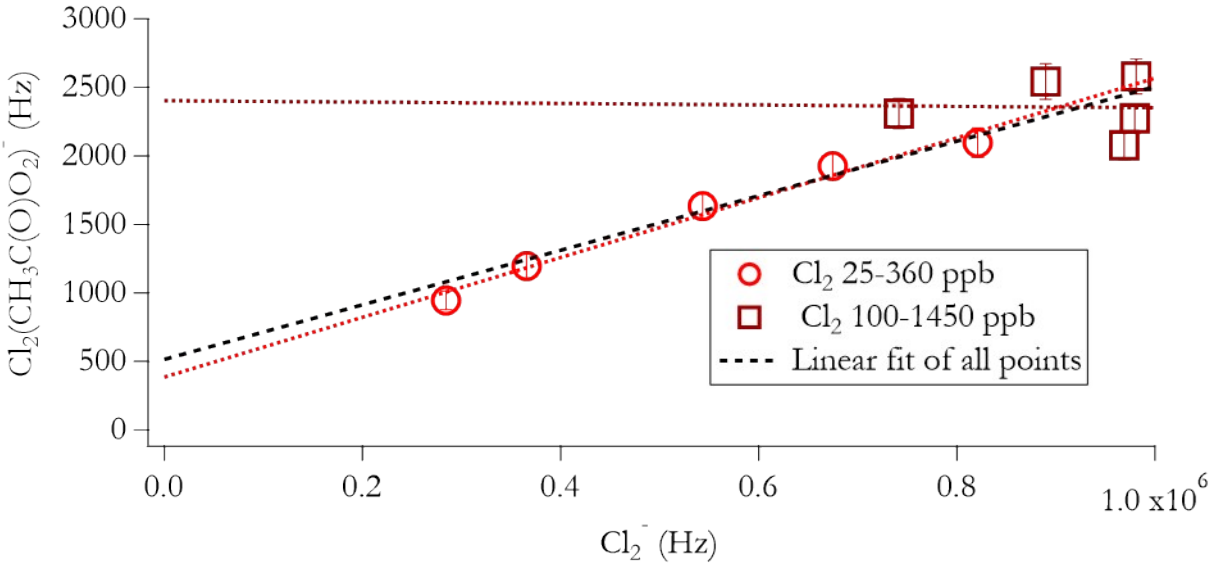

Figure S11. Observed relationship between $Cl_2(CH_3C(O)O_2)^-$ (produced by acetone photolysis) and Cl_2^- during alteration of the Cl_2 reagent gas mixture. 10 ppm Cl_2 cylinder (25-360 ppb Cl_2 in reagent gas mixture) data shown with light red circles and 40 ppm cylinder (100-1450 ppb Cl_2 in reagent gas mixture) data shown with dark red diamonds. Dotted lines are the linear least-squared fits to the 10 ppm and 40 ppm datasets, the black dashed line is the linear least-squared fit to the whole dataset. Cl_2 concentrations from the 40-ppm tank reflect those used for acid and ozone response in Figure 5 and Table S10. The non-linear relationship between Cl_2^- background counts and $Cl_2(CH_3C(O)O_2)^-$ signal here indicates that $Cl_2(CH_3C(O)O_2)^-$ was only directly dependent on Cl_2^- up to Cl_2 reagent gas concentrations of ca. 400 ppb. Past this concentration, it is possible that secondary chemistry in the IMR, perhaps involving reactions of Cl with $CH_3C(O)O_2$, diminishes observed sensitivity. Further testing of this reagent ion system is needed to stabilize and maximize Cl_2^- CIMS response to $RC(O)O_2$.

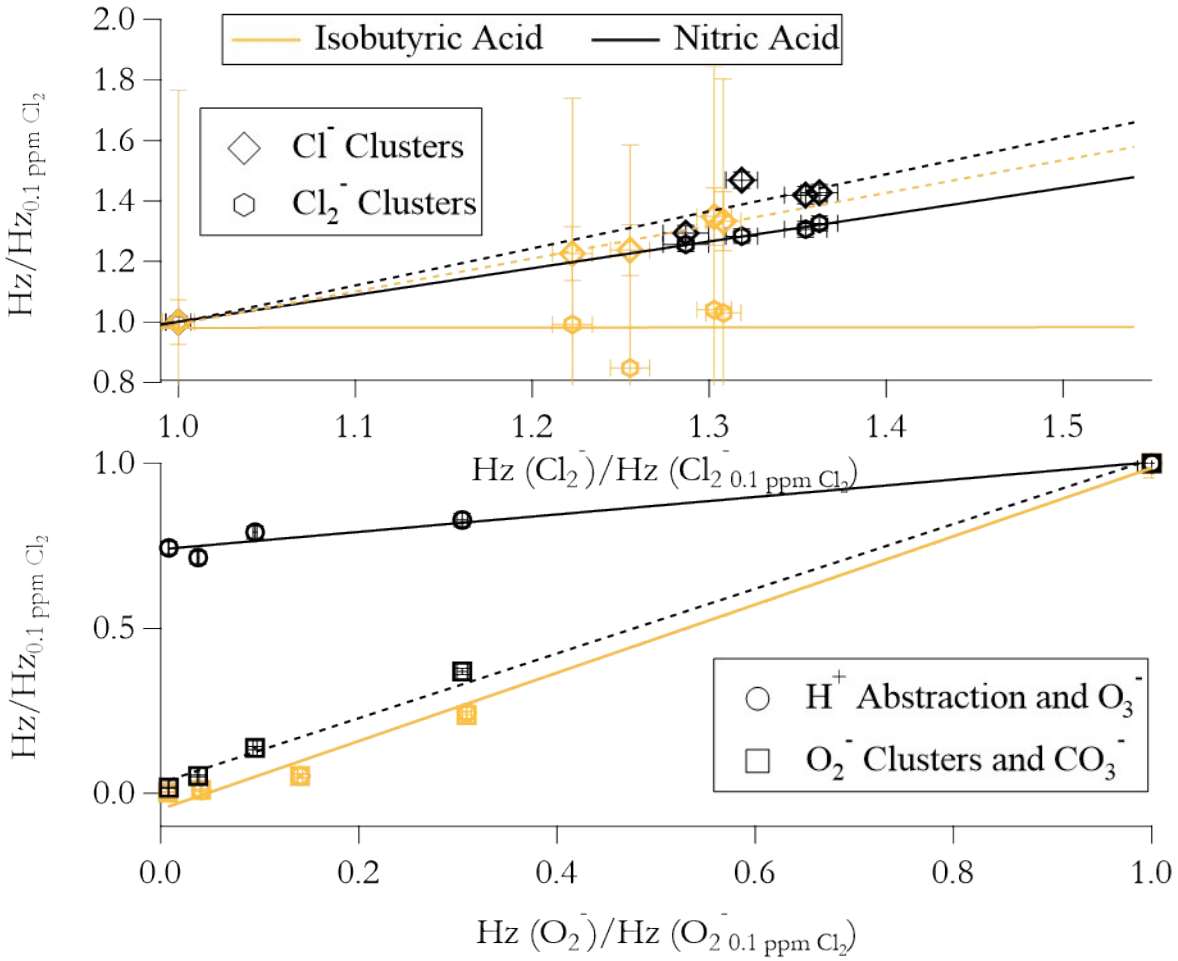

Figure S12. Analyte ion correlation plots for analytes not included in Figure 4.v. These are organized in the same manner as in main text Figure 5. Isobutyric acid was left off to improve readability of the graph. Isobutyric acid-Cl^- clusters behaved similarly to other organic acids. Cl_2^- cluster sensitivity was poor. We created an HNO_3 permeation tube, used identically to those described for organic acids. However, we did not calibrate the Cl_2-CIMS for HNO_3. HNO_3 was examined in this test for an expected reaction with Cl_3^- (see Amelynck et al. reference from main text). No HNO_3 product ion correlates clearly to Cl_3^-. dV scans (Figure S6) indicated that Cl_3^- was more tightly bound than any analyte ion, including those of HNO_3. Cl_3^- was less reactive than expected from limited literature information.

	Formic Acid	Acetic Acid	Propanoic Acid	Isobutyric Acid	Ozone
Ion	$HC(O)O^-$	$CH_3C(O)O^-$	$C_2H_5C(O)O^-$	$C_3H_7C(O)O^-$	CO_3^-
Reagent	O_2^-	O_2^-	O_2^-	O_2^-	O_2^-
Sensitivity	6.6 ± .2	38 ± 3	9.79 ± .06	5.98 ± .03	56 ± 4
Ion	$O_2(HC(O)OH)^-$	$O_2(CH_3C(O)OH)^-$	$O_2(C_2H_5C(O)OH)^-$	$O_2(C_3H_7C(O)OH)^-$	O_3^-
Reagent	O_2^-	O_2^-	O_2^-	O_2^-	O_2^-
Sensitivity	10.8 ± .2	98 ± 12	24.8 ± .2	13.6 ± .1	0.7 ± 0.7
Ion	$Cl(HC(O)OH)^-$	$Cl(CH_3C(O)OH)^-$	$Cl(C_2H_5C(O)OH)^-$	$Cl(C_3H_7C(O)OH)^-$	
Reagent	$Cl^- + Cl_2^-$	$Cl^- + Cl_2^-$	$Cl^- + Cl_2^-$	$Cl^- + Cl_2^-$	
Sensitivity	.41 ± .01	1.3 ± 0.1	.351 ± .001	.244 ± .009	
Ion	$Cl_2(HC(O)OH)^-$	$Cl_2(CH_3C(O)OH)^-$	$Cl_2(C_2H_5C(O)OH)^-$	$Cl_2(C_3H_7C(O)OH)^-$	
Reagent	Cl_2^-	Cl_2^-	Cl_2^-	Cl_2^-	
Sensitivity	1.10 ± 0.02	**0.025 ± 0.003**	**0.0552 ±0.006**	**0.024 ± 0.002**	

Table S13. Sensitivities (in ncps/ppt) for all organic acid and O_3 product ions normalized only using reagent ion signals that correspond to the associated ionizing reaction. In each section 'ion' denotes the measured product ion and 'reagent' provides the reagent ion, or sum of reagent ions, used for normalization. Normalized counts per second (ncps) are calculated per million corresponding reagent ion(s), as in the main text.